A PHOTOMETRIC AND KINEMATIC STUDY OF THE STARS AND INTERSTELLAR MEDIUM IN THE CENTRAL 2 KILOPARSECS OF NGC 3379[1]

MIRIANI G. PASTORIZA,[2,3] CLÁUDIA WINGE,[2,4] FABRICIO FERRARI,[2,4] F. DUCCIO MACCHETTO,[5,6] AND NICOLA CAON[7]

ABSTRACT

Hubble Space Telescope images of NGC 3379 show that the V and I luminosity profiles in the inner $13''$ of this E1 galaxy are represented by two different components: a stellar bulge following a Sérsic law with exponent $n = 2.36$ and a central core ($r < 0''.7$) with a characteristic "cuspy" profile. Subtraction of the underlying stellar component represented by the fitted Sérsic profile revealed the presence of a small ($r \approx 105$ pc) dust disk of about 150 $M_{\odot}$, oriented at P.A. = 125° and inclined $\approx 77°$ with respect to the line of sight. The same absorption structure is detected in the color index ($V - I$) image. The stellar rotation in the inner $20''$ is well represented by a parametric planar disk model, inclined $\approx 26°$ relative to the plane of the sky and with apparent major axis along P.A. $\approx 67°$. The gas velocity curves in the inner $5''$ show a steep gradient, indicating that the gas rotates much faster than the stars, although in the same direction. The velocity field of the gaseous system, however, is not consistent with the simple model of Keplerian rotation sustained by the large (7×10^9 $M_{\odot}$ within a radius of ~ 90 pc) central mass implied by the maximum velocity observed, but the available data preclude a more detailed analysis.

Subject headings: galaxies: elliptical and lenticular, cD — galaxies: individual (NGC 3379) — galaxies: ISM — galaxies: kinematics and dynamics — galaxies: photometry

1. INTRODUCTION

High spatial resolution images obtained with the *Hubble Space Telescope* (*HST*) revealed the presence of small nuclear stellar disks in several early-type galaxies (van den Bosch et al. 1994; van den Bosch, Jaffe, & van der Marel 1998) as well as patchy absorption due to dust near their nuclei (van Dokkum & Franx 1995). The presence of stellar disks in elliptical galaxies has important consequences on the mechanisms of galaxy formation since it suggests a continuity between spiral, lenticular, and elliptical galaxies, implying that a single mechanism may control the morphology of the protogalaxy (Bender et al. 1989; Capaccioli 1990). If, on the other hand, it is assumed that elliptical galaxies are formed by the merger of spiral galaxies (Illingworth & Franx 1989; Balcells & Quinn 1990; Hernquist & Barnes 1991) or coalescence of dwarf systems (Coté, Marzke, & West 1998), it is difficult to explain the survival of such small disks over large timescales after the merger event.

NGC 3379 is a bright E1 galaxy with almost perfectly elliptical isophotes (Lauer 1985). Detailed surface photometry based on photographic plates and CCD images covering the range from 18 to 29 mag arcsec^{-2} yielded a mean ellipticity of $\epsilon = 0.11$ and a major-axis mean position of P.A. = 70° (Capaccioli et al. 1990). The isophote twist is smaller than 5° and the ellipticity varies by less than 0.06 between $10''$ and $100''$ (Capaccioli et al. 1990; Peletier et al. 1990). The stellar rotation curves measured up to $R = 30''$ show evidence of slow (~ 50 km s^{-1}) rotation around the photometric minor axis (Franx, Illingworth, & Heckman 1989; Bender, Saglia, & Gerhard 1994) and a mean stellar velocity dispersion of 180 km s^{-1}. Higher velocity dispersion is observed in the galaxy core ($r \lesssim 2''$; Bender et al. 1994).

Although this galaxy is often regarded as the prototype for its morphological type, there have been several suggestions that it may actually be a face-on S0 galaxy (Capaccioli 1987; Nieto 1989) or at least a flattened elliptical (Strom et al. 1976; Statler 1994). Its intrinsic shape was found to be almost oblate in the inner $R/R_e < 0.4$ ($R_e \sim 54''$) region, with axial ratios of $b/a = 0.9$ and $c/a = 0.5$, and triaxial in the outer regions ($b/a = 0.75$ and $c/a = 0.5$) (Capaccioli et al. 1991, hereafter C91). These authors also remarked on the presence of a small stellar disk in the central regions of the galaxy. Combining photometric and kinematic data with dynamical models, Statler (1994) concluded that this object is in fact an elliptical galaxy, ruling out very flattened, triaxial shapes, but Statler & Smecker-Hane (1999, hereafter SS99), using more detailed stellar kinematic data, suggested that the two-dimensional velocity field of NGC 3379 indicates a two-component structure for the galaxy, with kinematical features closely resembling those seen in the rotation curve of the edge-on S0 galaxy NGC 3115.

Macchetto et al. (1996, hereafter Paper I) mapped the ionized gas of about 80 early-type galaxies using $H\alpha + $ [N II] narrowband imagery and found that NGC 3379 presents a small ($20'' \times 14''$) central disk of ionized gas with an estimated mass of 2.2×10^3 $M_{\odot}$ calculated from the $H\alpha$ luminosity. Recent high spatial resolution photometric and kinematic studies (Magorrian et al. 1998; van der Marel 1999) showed that this galaxy could harbor a central massive dark object (MDO) of $\sim 10^8$ $M_{\odot}$. The best-fitting three-integral models of Gebhardt et al. (1996) also indicate, besides the presence of a central MDO, that the intrinsic shape of the galaxy would be an E6 seen at an inclination of 27°.

In this work we address the stellar and gas kinematics and the dust morphology in the central 2 kpc of NGC 3379

[2] Instituto de Física-UFRGS, Av. Bento Gonçalves, 9500, C.P. 15051, CEP 91501-950, Porto Alegre, RS, Brazil.
[3] mgp@if.ufrgs.br.
[4] CNPq fellowship.
[5] Space Telescope Science Institute, 3700 San Martin Drive, Baltimore, MD 21218.
[6] Affiliated with the Astrophysics Division of ESA.
[7] Instituto de Astrofísica de Canarias, La Laguna, Tenerife, Spain.

using new spectroscopic observations taken as part of our program to study the interstellar medium in early-type galaxies as well as archival *HST* images. This paper is organized as follows. Section 2 presents the observations and data reduction. The luminosity profiles and dust distribution derived from *HST* images are discussed in § 3.1. The stellar kinematics are explored in § 3.2, where we test the simple case of disk rotation in a spherical potential, and the gas kinematics are discussed in § 3.3. The conclusions are summarized in § 4. To allow direct comparison with our previous results (Paper I; Ferrari et al. 1999), we adopt $H_0 = 55$ km s^{-1} Mpc^{-1}, and a distance to NGC 3379 of 14.5 Mpc, although a number of different values can be found in the literature (Sakai et al. 1997; Ciardullo, Jacoby, & Ford 1989). At this distance, $1''$ corresponds to 70 pc in the plane of the sky.[8]

2. OBSERVATIONS AND DATA REDUCTION

2.1. *The HST Images*

Archival *HST V* and *I* images were used to analyze in detail the photometric properties of the central ($r < 15''$) region of NGC 3379. The images were obtained with the Wide Field Planetary Camera 2 (WFPC2) + F555W and F814W filters, with the nucleus of the galaxy placed on the PC frame, resulting in a spatial scale of 0.046 arcsec pixel^{-1} and a resolution of $\sim0''.1$. The details of the observations are given in Table 1. Data reduction of the individual images followed the standard pipeline procedures for flat fielding and bias correction. The individual images for each filter (four images with the F555W and two with the F814W) were combined to remove cosmic rays, resulting in total exposure times of 1660 and 800 s for F555W and F814W final images, respectively. Those were then flux-calibrated in order to convert the F555W and F814W

***

[8] For a distance of 10–11 Mpc, the linear scale is 50 pc arcsec^{-1}, and the masses calculated in § 3.1 would be overestimated by a factor of 2.

TABLE 1
JOURNAL OF OBSERVATIONS—*HST*/WFPC2 IMAGES

Rootname	Filter	Exposure Time (s)
U2J20F01T.........	F555W	500
U2J20F02T.........		500
U2J20F03T.........		500
U2J20F04T.........		160
U2J20F05T.........	F814W	400
U2J20F06T.........		400

counts to the Johnson system at *V* and *I* (Biretta et al. 1996). The *V* and *I* *HST*-integrated magnitudes in a $10''$ aperture centered in the nucleus agree within 0.13 and 0.15 mag, respectively, with the ground-based data, implying very small uncertainties when deriving relative color maps of the galaxy. The final F555W and F814W images are shown in Figure 1.

2.2. *Spectroscopy*

To study the kinematics of the ionized gas detected in Paper I and to explore earlier suggestions about the presence of a stellar disk in the inner $30''$ of NGC 3379 (C91; SS99), long-slit spectra were obtained at position angles $70°$, $115°$, and $160°$, corresponding respectively to the major, intermediate, and minor axes of the gas distribution. The slit positions are shown in Figure 2, superimposed on the Hα + [N II] image and *R*-band isophotal map of NGC 3379 from Paper I.

The observations were conducted at the ESO 3.6 m telescope + EFOSC1 at La Silla, Chile. In order to maximize the coverage of the relevant stellar absorption and gaseous emission lines, we used the O150 grism in the range 5140–6900 Å with a dispersion of 3.4 Å pixel^{-1} and the CCD 26 (Tektronik 512×512 pixels) with a spatial scale of 0.61 arcsec pixel^{-1} and $\sim1''$ resolution. The slit width was set to
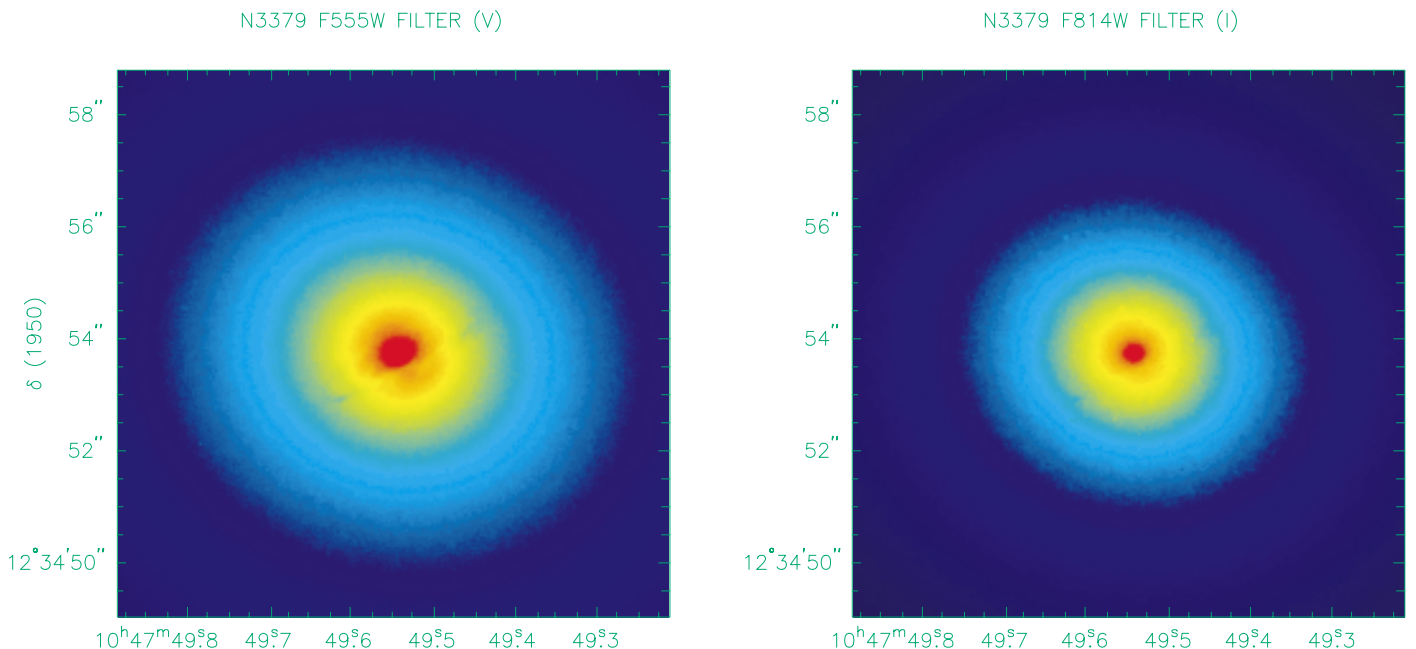

FIG. 1.—*HST*/WFPC2 *V* and *I* images of NGC 3379. Note the dust lane cutting across the inner $2''$ and the almost perfectly circular appearance of the outer regions. North is up and east is to the left.
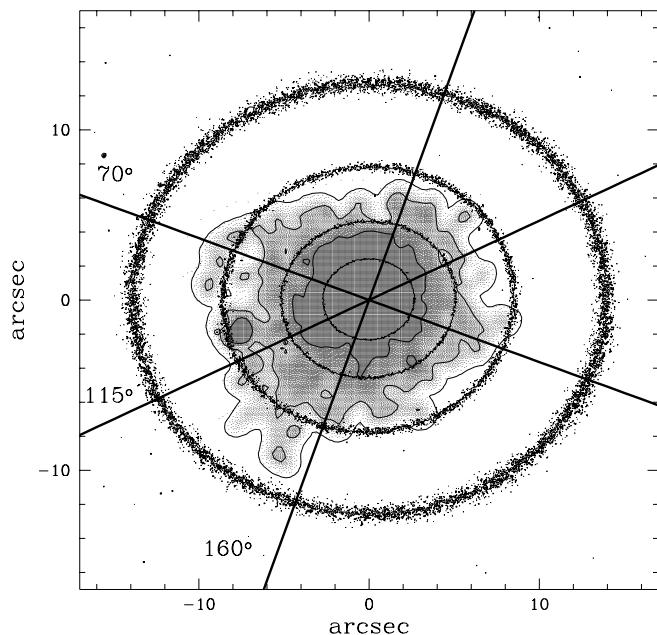
FIG. 2.—Observed slit positions superimposed on the Hα+[N II] image from Macchetto et al. (1996) and *V*-band isophotes map from the *HST* image. Orientation is the same as in Fig. 1.

1″ with a useful length of 3′. The observational procedure was to obtain two exposures of 40–45 minutes at each position angle in order to increase the signal-to-noise ratio and facilitate the removal of cosmic rays. The observations are summarized in Table 2. The stability of the instrument has been checked by comparing the position of the sky emission lines present in the galaxy spectra, and we found that the relative shift is always less than 0.2 pixels, with an rms of about 0.1 pixels ($\sim$17 km s^{-1}). We also verified the correct alignment of the CCD *y*-axis with the dispersion direction by tracing, for each spectrum, the position of the centroid of the galaxy or starlight distribution along each detector row. No systematic misalignment was found, with the tilts never larger than 0″.05 (0.5 pixels). Several kinematic (giant stars in the spectral type range K0–K4 III, with rotation velocity less than 20 km s^{-1}) and spectrophotometric standards were observed at the beginning and the end of each night.

TABLE 2
JOURNAL OF OBSERVATIONS—ESO SPECTRA

Object	Position Angle (deg)	Exposure Time (s)
NGC 3379......	70	2 × 2700
	115	2 × 2700
	160	2 × 2700
Kinematic Standards		
HR 2305........	Parallactic angle	1
HR 3110........	Parallactic angle	1
HR 25074	Parallactic angle	1
HR 3122........	Parallactic angle	1
Spectrophotometric Standards		
LTT 7379.......	Parallactic angle	120
EG 274	Parallactic angle	180
LTT 7987.......	Parallactic angle	180

The data reduction was carried out the usual way, using IRAF[9] tasks. The mean bias level was subtracted and the frames were divided by a normalized dome flat field to remove pixel-to-pixel variations. The averaged sky flat was used to correct for the nonuniformity of the response along the slit. Wavelength calibration was obtained by fitting a low-order polynomial to the centroid of the brightest, nonsaturated lines in the HeAr comparison lamp spectra, with residuals of less than 0.15 Å. Relative velocities were measured with an uncertainty of $\sim$5 km s^{-1}.

A cross-correlation algorithm, working in pixel space, has been used to derive the stellar kinematics (Dalle Ore et al. 1991). Briefly, the continuum of the galaxy and template star spectra were fitted with a polynomial of order $\sim$20 and subtracted. Each resulting galaxy spectrum was then cross-correlated with that of the kinematic template star, and the center of a Gaussian fitted to the central peak of the correlation function gives the radial velocity of the galaxy with respect to the template star.

3. RESULTS

3.1. *Luminosity Profiles and V − I Image*

Elliptical galaxies have central surface brightness distributions of two distinct types: those with steep profiles that do not show a break in the slope—called "power-law" galaxies—and those that do show a break at a given radius r_b, from a steeper outer profile to a flatter core—called "core" galaxies (Lauer et al. 1992, 1995; Crane et al. 1993; Ferrarese et al. 1994; Forbes, Franx, & Illingworth 1995; Faber et al. 1997). NGC 3379 was classified by Faber et al. (1997) as a "core"-type galaxy, and in addition to the characteristic luminosity profiles, we found that the *HST V* and *I* images reveal a well-defined nuclear dust structure (see Fig. 1) similar to that observed in the E2 galaxy NGC 6251 (Ferrarese & Ford 1999). The presence of such a nuclear dust disk raises the possibility that the observed central luminosity profile could be altered by absorption, creating an artificial break and mimicking a "core"-type profile. To analyze the role that the dust plays on the luminosity profile, we carried out detailed surface photometry of the central region of NGC 3379 using the IRAF task ELLIPSE to measure the main isophotal parameters (position angle, ellipticity, and Fourier coefficient c_4). The fitting results are shown in Figure 3 as a function of the distance *a* in arcseconds along the isophotal major axis.

The position angle of the major axis presents an almost constant value of 75° between 2″ and 13″, decreasing slightly to 70° for larger distances. Within the inner 2″, on the other hand, the P.A. changes considerably, first decreasing to lower values of up to 50° at $a \sim 1″$ and then increasing again to reach a value of P.A. = 120° at 0″.4, which is close to the orientation of the dust disk's major axis. The isophotes external to 5″ show a constant ellipticity with a value of 0.12, but internal to this radius the ellipticity increases to up to 0.24 at 0″.5. It is very significant that the changes in both the P.A. of the major axis and the ellipticity of the isophotes start at approximately 2″, in close correspondence with the presence of the dust disk.
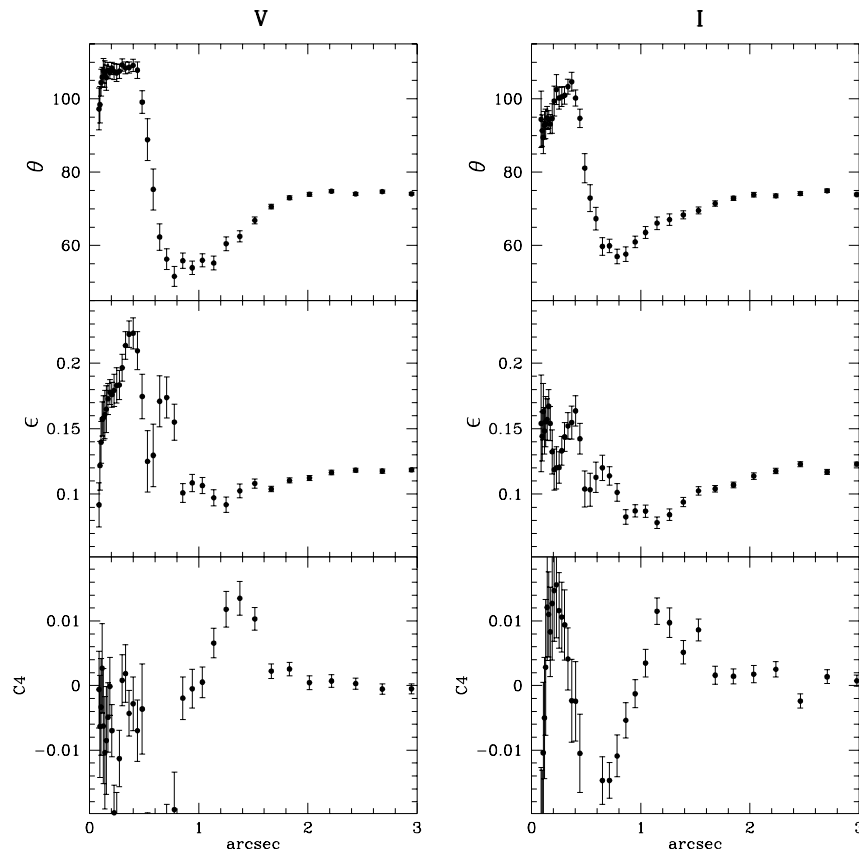

FIG. 3.—Results of the isophote fitting as a function of the distance along the major axis a in arcseconds. *Top to bottom*: position angle of the major axis, ellipticity, and Fourier c_4 parameter.

The c_4 parameter is related to the shape of the isophotes: elliptical galaxies with "core" profiles tend to present "boxy" isophotes ($c_4 < 0$), while "power-law" galaxies tend to be more disklike ($c_4 > 0$) (Nieto, Bender, & Surma 1991). In NGC 3379, the c_4 parameter external to $2''$ assumes an almost constant value of zero, while internal to this radius it first rises to positive values up to $a \sim 1\rlap{.}''2$ and then oscillates around zero in the innermost regions. Such behavior indicates that, outside the region where the dust disk is present, this galaxy has indeed almost perfectly elliptical isophotes, and that the dust affects the very inner isophotes making them appear more disklike where they would be expected to be "boxy" based on the classification of NGC 3379 as a "core" galaxy (Faber et al. 1997; Kormendy 1999).

The derived V and I luminosity profiles along the major axis at P.A. $= 70°$ show evidence of a change in slope at $r \sim 0\rlap{.}''7$. In order to verify if this depression could be attributed to the presence of the dust disk, we performed the ELLIPSE fitting with the region occupied by the disk masked-out and found the same profiles as in the previous case (without masking). Therefore, the presence of dust has a negligible effect on the profiles. The change in the profile slope makes it necessary to use two different laws for the fitting; from $0\rlap{.}''08$ to $0\rlap{.}''68$, where the profiles are shallower, a cuspy law was used:

$$I = I_0 r^{-\gamma} ,$$

$$\mu - \mu_0 = -\gamma \log r ; \qquad (1)$$

from $0\rlap{.}''68$ to $15''$, the Sérsic law (Sérsic 1968) provides a better fit:

$$I(r) = I_n \exp \left\{ - b_n \left[\left(\frac{r}{r_n} \right)^{1/n} - 1 \right] \right\} ,$$

$$b_n = 0.868n - 0.142 . \qquad (2)$$

The resulting parameters of the fit are shown in Table 3.

Figure 4 shows the observed (*star symbols*) and fitted (*solid line*) profiles from the V image. The interval $0\rlap{.}''7 \lesssim r \lesssim 9''$ is well reproduced by a Sérsic law with index $n = 2.36$, indicating that the profile is more concentrated than the usual de Vaucouleurs light distribution, which fails to reproduce the observed luminosity. The very inner region ($r < 0\rlap{.}''7$) is expanded in the zoomed insert to the right,

TABLE 3

PHOTOMETRIC PARAMETERS

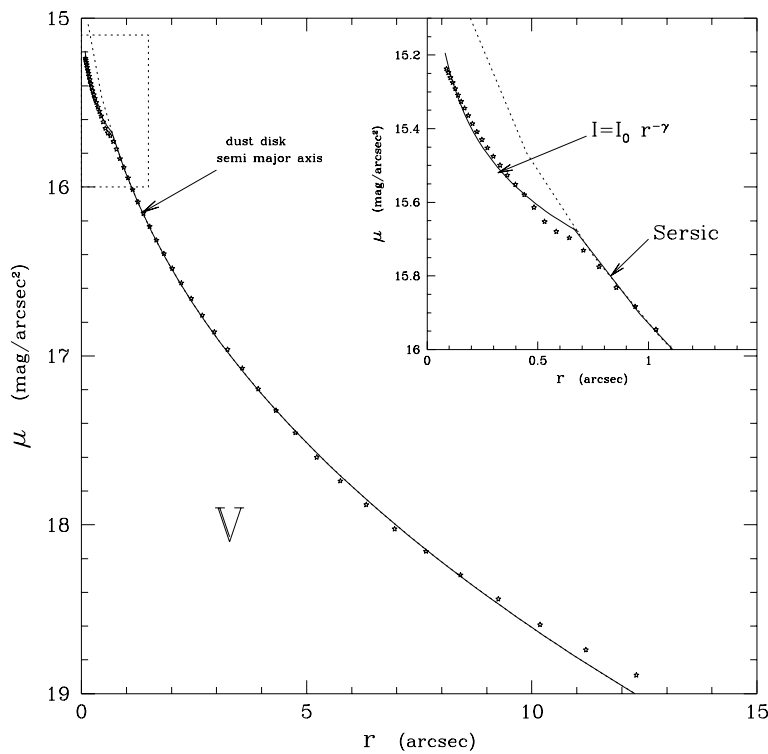| Parameter	V	I
Cuspy Law		
I_0 (mag)	15.05 ± 0.02	12.98 ± 0.02
γ	0.210 ± 0.004	0.203 ± 0.005
Sérsic Law		
I_e (mag)	19.1 ± 0.1	17.0 ± 0.2
r_e (arcsec)	12.7 ± 0.5	12.4 ± 0.6
n	2.36 ± 0.05	2.39 ± 0.07

Fig. 4.—Luminosity profile decomposition for the *HST V* image. The insert to the right shows an expanded view of the central 1″5, where the "cuspy" law dominates.

where it can be clearly seen where the Sérsic law breaks up and the nuclear profile dominates.

The fitted Sérsic profile was assumed to represent the stellar light distribution for $r \lesssim 10''$, and a model image was built using the IRAF task BMODEL. This model was then subtracted from the *V* image and the result is shown in the left panel of Figure 5. For $r \lesssim 0''7$, where the "cuspy" law dominates, the nuclear core appears now very clearly in absorption, since its profile is $\simeq 0.2$ mag fainter than the external profile extrapolation. The subtraction also reveals

a very conspicuous dust structure at $r \simeq 1''5$, reminiscent of the dust disk seen in NGC 6251 (Ferrarese & Ford 1999). The $V - I$ color index image, shown in the right panel of Figure 5, confirms the presence of a dust disk with major and minor axes $3''$ and $0''8$ long, respectively, with the major axis oriented along P.A. $\approx 125°$. Assuming that the disk is circular, the observed axial ratio implies an inclination of $77°$ between the line of sight and the normal to the disk.

From our data, we measured a mean A_V extinction of 0.11 mag inside the disk. Assuming that the dust is in a
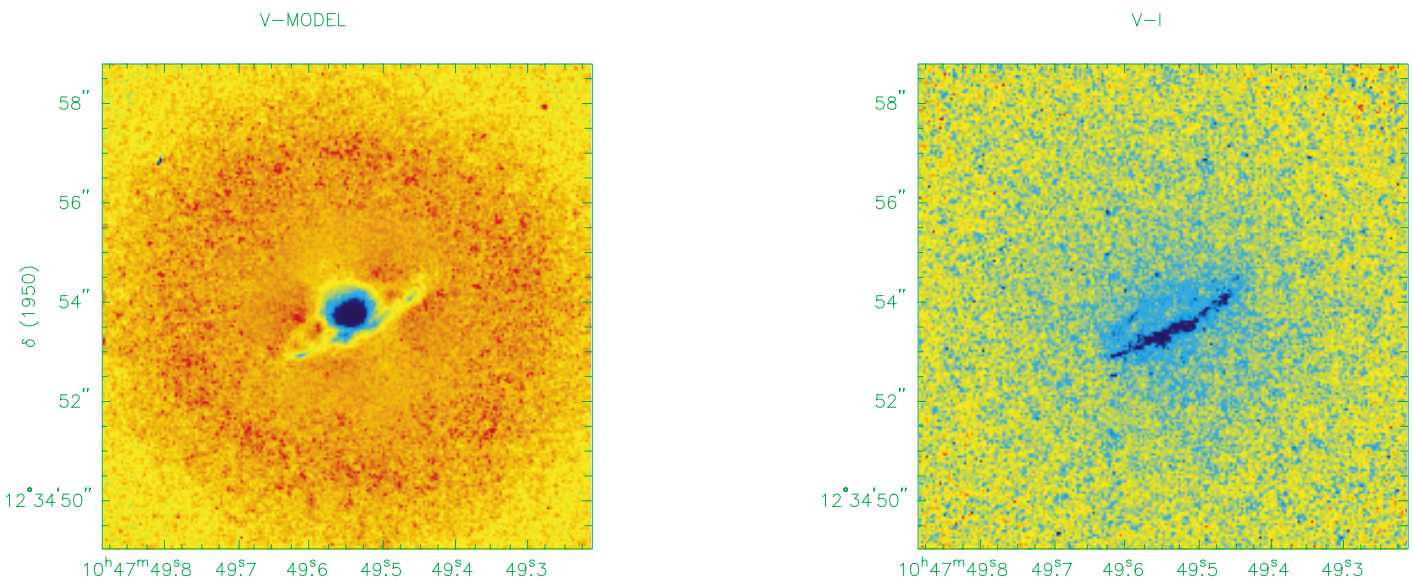

Fig. 5.—*Left*: *HST V* image after the subtraction of the bulge model as described in the text. Note the central cusp, where the luminosity profile is fainter than the Sérsic law, and the dust ring with $r \sim 1''5$. *Right*: $V - I$ color index image. Only the dust ring is visible, evidence that the central cusp is not an effect of localized absorption. Orientation as in Fig. 2.

uniform layer with $r \simeq 1\farcs5$ (105 pc) and is composed mainly of silicate grains with mean size 0.08 μm, a dust mass of 150 $M_\odot$ was estimated following the method discussed in Ferrari et al. (1999). The analysis in that paper also indicated the presence of a more extended, asymmetric dust cloud extending about 5″ to the south, with an estimated mass of ~ 100 $M_\odot$ and mean A_V extinction of 0.027 mag. The much larger mass and extinction measured in the disk over that of the southern extended dust cloud indicates the presence of a dust gradient toward the central regions of the galaxy.

The fit of the I-band luminosity profile yields very similar results, as can be seen in Table 3 and Figure 6. Since the I band should be less affected by reddening, the presence of the central cusp in the I profile shows that absorption by dust cannot be the primary cause for the observed change of slope. The isophotal parameters discussed above indicate that dust indeed plays a role in distorting the inner isophotes, but it is not a strong enough effect to modify the global luminosity profiles.

This galaxy therefore presents a characteristic "cuspy" core, with the steeper outer (Sérsic) profile breaking up at $r_b \approx 0\farcs7$ to be replaced by a shallower inner profile, given by equation (1) with $\gamma = 0.21$. Note that the profile break is located about $0\farcs8$ from the most absorbed part of the dust disk, and therefore the light depletion observed in the luminosity profile cannot be explained by dust absorption since it is not present where this is stronger. This same conclusion is reinforced by the $V-I$ color index image (Fig. 5), where only the dust ring is visible, evidence that the central cusp is not an effect of localized absorption.

Several models have been proposed to account for core formation, such as (a) an isothermal sphere with density profile r^{-2}; (b) black holes (BH) adiabatically grown in homogenous isothermal cores (Young 1980; van der Marel

1999); (c) the orbital decay of massive black holes accreted in mergers, where the decaying BHs may heat and eject stars from the center, eroding the power law if any exists and creating a core (Faber et al. 1997 and references therein); or (d) remnants formed by mergers of disk galaxies, where the dissipation in the gas and ensuing star formation during the merger process leaves a dense stellar core in the remnant (Mihos & Hernquist 1994). These last models can account for the extra light at a small radius (over a Sérsic law or de Vaucouleurs functions) in the luminosity profile of "power-law"–type galaxies (Kormendy 1999) but cannot reproduce the broken light profile observed in NGC 3379, which is fainter than the Sérsic distribution in the inner region.

Magorrian et al. (1998) constructed dynamical models for a sample of 36 early-type galaxies, including NGC 3379, using HST photometry and ground-based kinematic data. The models assume that the galaxies are axisymmetric, described by a two-integral distribution function with an arbitrary inclination angle, a position-independent stellar mass-to-light ratio, and a central MDO of arbitrary mass. Such an approach was able to provide acceptable fits to 32 galaxies in the sample, and a model with an MDO mass of 3.9×10^8 $M_\odot$ and a mass-to-light ratio Υ of 5.3 was found to be an adequate description for the stellar kinematics of NGC 3379. In a similar approach, Gebhardt et al. (1996) used axisymmetric, three-integral models to fit both $HST/$ Faint Object Spectrograph and ground-based spectroscopy along the major and minor axes. $HST/$WFPC2 and ground-based images were used to constrain the light distribution. The best-fit model for NGC 3379 also required the presence of a central MDO with mass of 6×10^8 $M_\odot$.

Recently, van der Marel (1999), studying the models first proposed by Young (1980) of adiabatically grown black holes, predicted that the luminosity profiles should behave
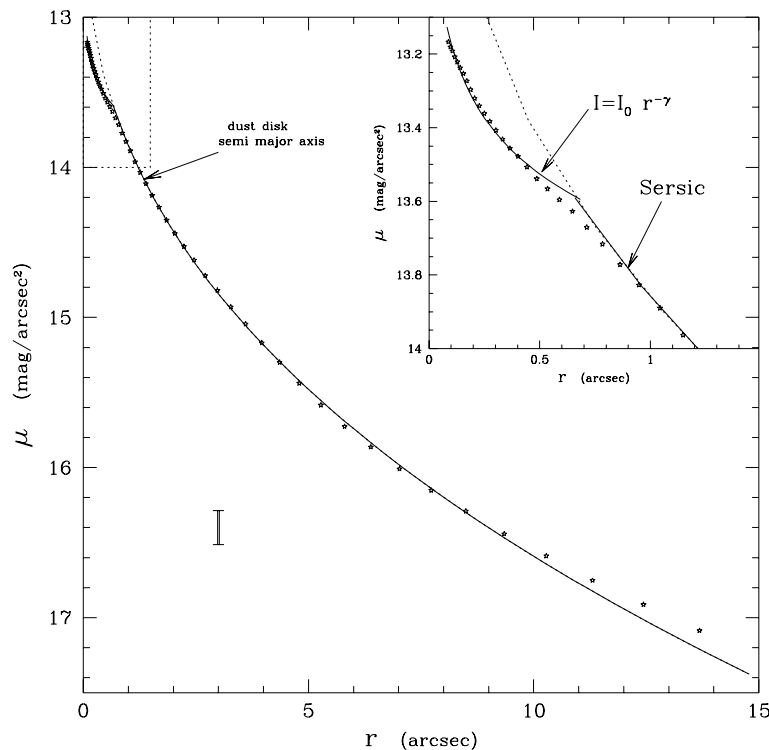

FIG. 6.—Luminosity profile decomposition for the HST I image

as $I = r^{-1/2}$ for asymptotically small radii, but as $I = r^{-\gamma}$ at radii observable with *HST*, with the index γ increasing monotonically with the mass of the central object. The index γ can assume all the observed values and therefore, both "core" and "power-law" profiles can be reproduced. Within this approach, the luminosity profile of NGC 3379 can be reproduced with the inclusion of a central black hole with mass of $1.9 \times 10^8 \, M_\odot$.

3.2. *Stellar Kinematics: An Inner Disk?*

In this section, we use the spectroscopic data described in § 2.2 to explore the possible presence of a stellar disk as well as to study the kinematics of the ionized gas shown in Paper I. The observed stellar rotation curves are presented in Figure 7. In agreement with previous results (Franx at al. 1989; Bender et al. 1994; SS99), it can be seen that the galaxy shows a fairly symmetric rotation curve along P.A. = 70° and 115°, with a steeper velocity gradient observed in the inner 6″. The rotation curve along P.A. = 160° is almost flat, confirming once more the presence of rotation around the galaxy's minor axis. The kinematic breaks remarked by SS99 at ∼5″ are also clearly discernible in our data.

To model the stellar kinematics, we assumed that the stars follow circular orbits in a plane and used Bertola et al.'s (1991) analytic expression as a first-order approx-

imation for the observed rotation curve:

$$V_c(r) = \frac{AR}{(R^2 + C_o^2)^{p/2}} + V_{sys} , \qquad (3)$$

where V_{sys} is the systemic velocity, R is the radius in the plane of the disk and A, C_o, and p are parameters that define the amplitude and shape of the curve. If $v(r, \Psi)$ is the observed radial velocity at a position (r, Ψ) in the plane of the sky, where r is the projected radial distance from the nucleus and Ψ is its corresponding position angle, we have

$$v_{mod}(r, \Psi) = V_{sys} + \frac{Ar \cos(\Psi - \Psi_o) \sin i \cos^p i}{(r^2\eta + C_o^2 \cos^2 i)^{p/2}} , \qquad (4)$$

with

$$\eta \equiv [\sin^2(\Psi - \Psi_o) + \cos^2 i \cos^2(\Psi - \Psi_o)] ,$$

where i is the inclination of the disk ($i = 0$ for a face-on disk) and Ψ_o is the position angle of the line of nodes.

The stellar rotation curves for P.A. = 70°, 115°, and 160° described above were combined with the data from Franx et al. (1989) for P.A. = 68° and 158°, and from SS99 for P.A. = 25°, 70°, 115°, and 340°. Our data agree very well with the rotation curves given by SS99 along the same P.A.s (see Fig. 8). The various parameters were determined simul-
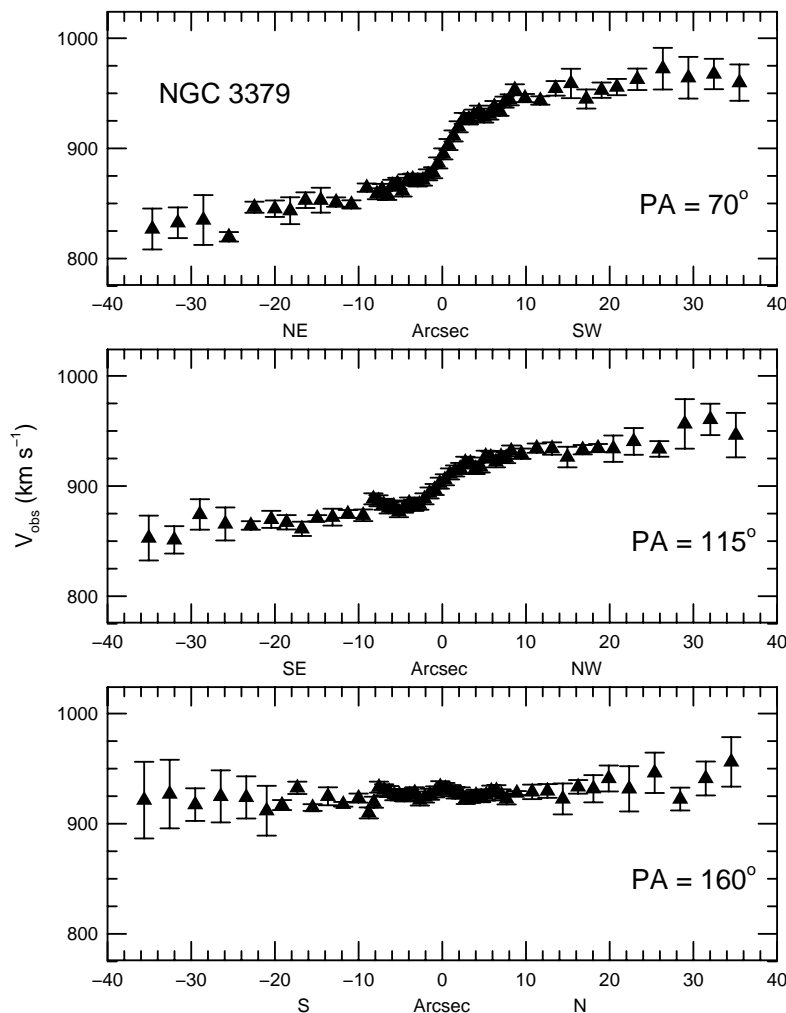

FIG. 7.—Observed rotation curves for P.A. = 70°, 115°, and 160°
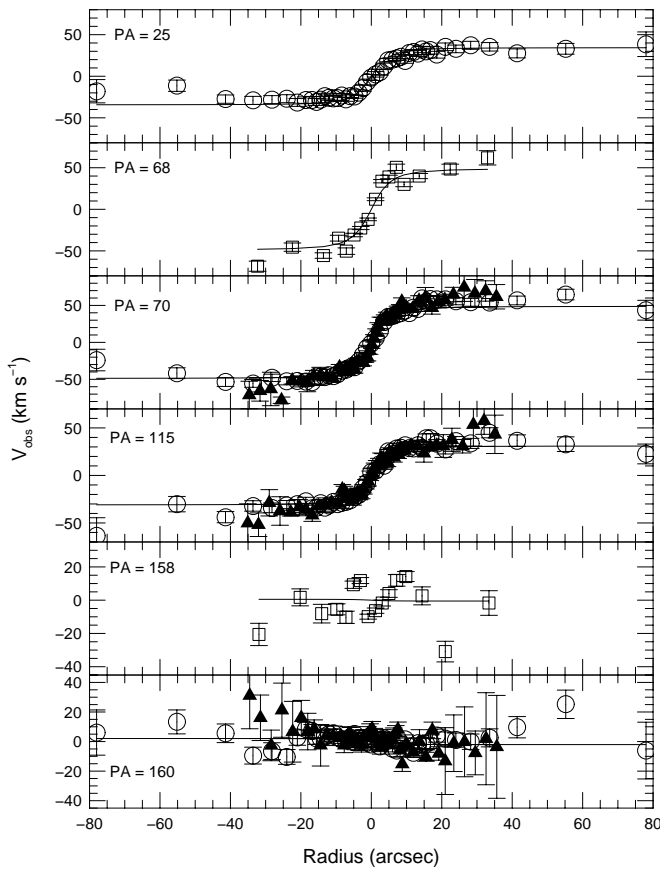
FIG. 8.—Observed stellar rotation curves and the resulting planar disk model fit (*solid line*). The filled triangles represent the data presented in this paper, open squares are the data from the two position angles published by Franx et al. (1989), and the open circles represent the data from SS99.
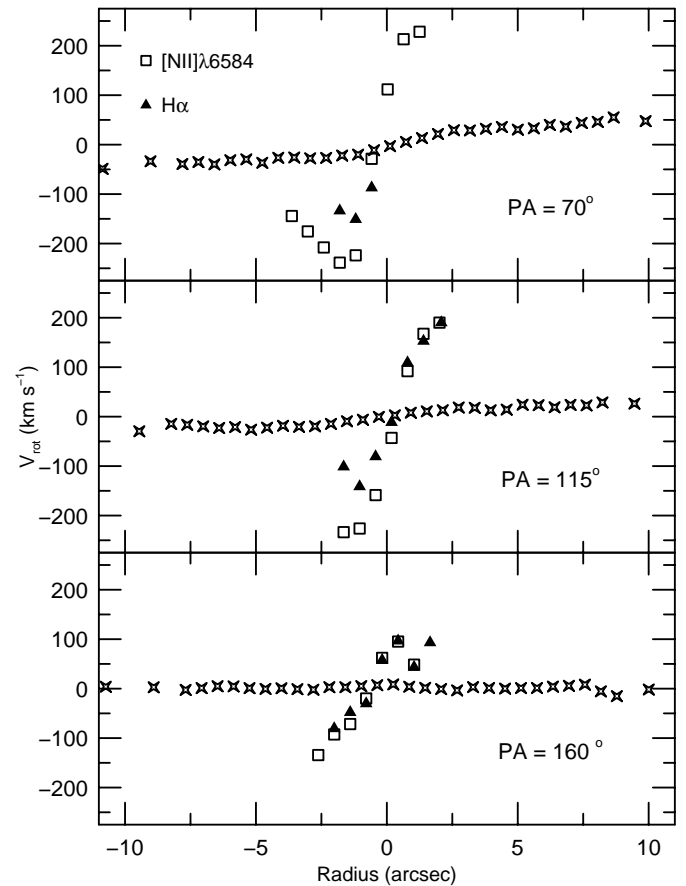

FIG. 9.—Observed emission-line rotation curves ([N II], *open squares*; Hα, *filled triangles*), superimposed on the correspondent stellar rotation curves (*star symbols*). Note the much higher velocity of the gas.

taneously by minimizing the residuals $\Delta v = v_{obs} - v_{mod}$, with $v_{mod}(r, \Psi, A, C_o, p, i)$ and $v_{obs}(r, \Psi)$ being the model and observed radial velocities, respectively, at the position (r, Ψ) in the plane of the sky.

We used a Levenberg-Marquardt nonlinear least-squares algorithm to fit the above model. The data from the nine sets were first fitted with A, C_o, p, Ψ_o, i, and V_{sys} as free parameters, with V_{sys} having the same value for all data points (except for SS99, where V_{sys} was initially set to zero). Then, to take into account possible zero-point velocity offsets between the data sets, each one was separately fitted allowing V_{sys} to vary but keeping the remaining parameters fixed to the values obtained before. The resulting systemic velocity for each set was subtracted from the observed values and all data were refitted with A, C_o, p, Ψ_o, and i as free parameters. Finally, the effect of the initial guess on the parameters was explored running a Monte Carlo search for a wide interval of values for each parameter, while the others were given their best-fit values as the initial guess. An unstable fit will show as a large deviation from the original model.

The best solution (see Table 4 and solid line in Fig. 8) corresponds to an asymptotically flat rotation curve. The model is a good representation for the data up to $R \sim 20''$ and indicates that the stellar disk is inclined $\approx 26°$ relative to the plane of the sky, with the apparent major axis located at P.A. $\approx 67°$. These values are in very good agreement with

the V and I isophotal parameters analyzed in § 3.1, where it was shown that the P.A. of the major axis has an almost constant value of 75° between 2″ and 13″, converging to 70° for larger distances, and the ellipticity of the isophotes external to 5″ has a constant value of 0.119, which (assuming that the isophotal contours originate in a circular stellar disk) imply an inclination of $\approx 28°$. Our results are also in agreement with the parameters derived photometrically by C91. The observed deviation of the data points from the planar rotation model at larger radii is also expected within C91's analysis, where the triaxiality of the bulge grows outward and our model of purely planar rotation cannot represent the more complex stellar velocity field. We stress that our analysis does not *prove* the existence of a stellar disk in NGC 3379. It shows that such a disk is indeed a plausible first-order representation, but

TABLE 4
KINEMATICAL PARAMETERS

Parameter	Model
A (km s^{-1})......	113 (110–117)
p	1.0
C_o (arcsec)	5.8 (5.7–5.9)
Ψ_o (deg)	67 (67–72)
i (deg)	26 (25–28)

with the limited spatial resolution of ground-based observations it is not possible to fully deconvolve the triaxial motions of an elliptical or bulge system and show that a planar disk is the *only* possible model for the observed stellar kinematics.

3.3. *Gas Kinematics*

To analyze the gas kinematics, we have used the Hα + [N II] λ6584 emission lines which are the only ones detected in our data. The underlying stellar continuum was obtained by integrating the spectra outside the line-emitting region and was then subtracted from the central rows. The gas velocity was measured by interactively fitting a single Gaussian component to the emission lines in each individual spectrum. Reliable measurements were obtained in only the inner 5″, corresponding to approximately half the extension of the ionized gas region detected in Paper I. The gas velocities along the three observed positions are shown in Figure 9, superimposed on the stellar rotation curves.

In the inner 5″, the observed velocities are up to ~ 240 km s^{-1} at P.A. = 70°, and up to ~ 210 km s^{-1} at P.A. = 115°; a smaller rotation ($\Delta v \sim 90$ km s^{-1}) is still observed at P.A. = 160°. The steeper gradient of the gas rotation curves indicates that it rotates much faster than but in the same direction as the stars. Since similar maximum rotational velocities are observed at both P.A. = 70° and 115°, we can quite safely assume that the position angle of the major axis of the gas disk would be approximately halfway, namely, at P.A. $\sim 85°$. Assuming that the gas is indeed in a disk, the axial ratio derived from the isophotal fitting in the Hα + [N II] image implies a inclination i of 25°. Using these two values for the projection angles, the deprojected velocity of the gas at $r = 1.\!''3$ (91 pc) is ~ 580 km s^{-1}. If the gas was in pure Keplerian rotation, this value would imply that the total mass inside this radius is $\sim 7 \times 10^9$ $M_\odot$. Therefore, a quite large gravitational

mass would be required inside the inner 2″ in order to support the gas rotation. The limited amount of data, however, precludes a more detailed analysis.

4. CONCLUSIONS

From our analysis of archival V and I *HST* images and ground-based spectra of NGC 3379, we conclude the following:

1. The V and I luminosity profiles in the inner 13″ cannot be represented by a single component, with the fitting revealing two different systems: the external one following a Sérsic law with an $n = 2.36$ index, and therefore steeper than the usual de Vaucouleurs $r^{-1/4}$ profile; and a central core ($r < 0.\!''7$) with a characteristic "cuspy" profile.

2. The $V - I$ color index image and the subtraction of the underlying stellar component represented by the fitted Sérsic profile from the V image revealed the presence of a small ($r \sim 105$ pc) dust disk, oriented at P.A. $\sim 125°$ and inclined $i \sim 77°$ with respect to the line of sight, with mass ~ 150 $M_\odot$.

3. The stellar rotation in the inner 20″ can be quite well described by a parametric disk model. The model indicates that the disk is inclined $\sim 26°$ relative to the sky plane, with the apparent major axis located at P.A. $\sim 67°$. While our analysis does not unambiguously demonstrate the existence of a stellar disk in NGC 3379, it shows that within the limitations of the data, rotation in a planar disk is a plausible fit to the observed stellar rotation curves.

4. The gas in the inner 5″ rotates in the same direction as the stars, although much faster.

REFERENCES

Balcells, M., & Quinn, P. J. 1990, ApJ, 361, 381
Bender, R., Capaccioli, M., Macchetto, F. D., & Nieto, J.-L. 1989, Messenger, 55, 6
Bender, R., Saglia, R. P., & Gerhard, O. E. 1994, MNRAS, 269, 785
Bertola, F., Bettoni, D., Danziger, J., Sadler, E., Sparke, L., & de Zeeuw, T. 1991, ApJ, 373, 369
Biretta, J. A., et al. 1996, WFPC2 Instrument Handbook (version 4.0; Baltimore: STScI)
Capaccioli, M. 1987, in IAU Symp. 127, Structure and Dynamics of Elliptical Galaxies, ed. T. de Zeeuw (Dordrecht: Reidel), 47
———. 1990, in Bulges of Galaxies, ed. B. Jarvis & D. M. Terndrup (Garching: ESO), 231
Capaccioli, M., Held, E. V., Lorenz, H., & Vietri, M. 1990, AJ, 99, 1813
Capaccioli, M., Vietri, M., Held, E. V., & Lorenz, H. 1991, ApJ, 371, 535 (C91)
Ciardullo, R., Jacoby, G. H., & Ford, H. C. 1989, ApJ, 344, 715
Coté, P., Marzke, R. O., & West, M. J. 1998, ApJ, 501, 554
Crane, P., et al. 1993, AJ, 106, 1371
Dalle Ore, C., Faber, S. M., Jesus, J., Stoughton, R., & Burstein, D. 1991, ApJ, 366, 38
Faber, S. M., et al. 1997, AJ, 114, 1771
Ferrarese, L., & Ford, H. C. 1999, ApJ, 515, 583
Ferrarese, L., van den Bosch, F. C., Ford, H. C., Jaffe, W., & O'Connell, R. W. 1994, AJ, 108, 1598
Ferrari, F., Pastoriza, M. G., Macchetto, F. D., & Caon, N. 1999, A&AS, 136, 269
Forbes, D. A., Franx, M., & Illingworth, G. D. 1995, AJ, 109, 1988
Franx, M., Illingworth, G. D., & Heckman, T. 1989, ApJ, 344, 613
Gebhardt, K., Richstone, D., Kormendy, J., Bender, R., Faber, S., Lauer, T., Magorrian, J., & Tremaine, S. 1996, BAAS, 189, 111.03
Hernquist, L., & Barnes, J. E. 1991, Nature, 354, 210

Illingworth, G. D., & Franx, M. 1989, in Dynamics of Dense Stellar Systems, ed. D. Merrit (Cambridge: Cambridge Univ. Press), 13
Kormendy, J. 1999, in Galaxy Dynamics, ed. D. R. Merrit, M. Valluri, & J. A. Sellwood (San Francisco: ASP), 124
Lauer, T. R. 1985, MNRAS, 216, 429
Lauer, T. R., et al. 1992, AJ, 103, 703
———. 1995, AJ, 110, 2622
Macchetto, F. D., Pastoriza, M. G., Caon, N., Sparks, W. B., Giavalisco, M., Bender, R., & Capaccioli, M. 1996, A&AS, 120, 463 (Paper I)
Magorrian, J., et al. 1998, AJ, 115, 2285
Mihos, J. C., & Hernquist, L. 1994, ApJ, 437, L47
Nieto, J.-L. 1989, in Proc. Second Extragalactic Astronomy Regional Meeting in Cordoba, Argentina (Cordoba: Academia de Ciencias), 239
Nieto, J.-L., Bender, R., & Surma, P. 1991, A&A, 244, L25
Peletier, R. F., Davies, R. L., Davis, L. E., Illingworth, G. D., & Cawson, M. 1990, AJ, 100, 1091
Sakai, S., Madore, B. F., Freedman, W. L., Lauer, T. R., Ajhar, E. A., & Baum, W. A. 1997, ApJ, 478, 49
Sérsic, J. L. 1968, Atlas de Galaxias Australes (Cordoba: Univ. Cordoba), 141
Statler, T. S. 1994, AJ, 108, 111
Statler, T. S., & Smecker-Hane, T. 1999, AJ, 117, 839 (SS99)
Strom, S. E., Strom, K. M., Goad, J. W., Vrba, F. J., & Rice, W. 1976, ApJ, 204, 684
van den Bosch, F. C., Ferrarese, L., Jaffe, W., Ford, H. C., & O'Conell, R. W. 1994, AJ, 108, 1579
van den Bosch, F. C., Jaffe, W., & van der Marel, R. P. 1998, MNRAS, 293, 343
van der Marel, R. P. 1999, AJ, 117, 744
van Dokkum, P. G., & Franx, M. 1995, AJ, 110, 2027
Young, P. 1980, ApJ, 242, 1232